Chaos

Competitive interplay of repulsive coupling and cross-correlated noises in bistable systems

Cite as: Chaos **31**, 061106 (2021); https://doi.org/10.1063/5.0056173
Submitted: 07 May 2021 • Accepted: 25 May 2021 • Published Online: 07 June 2021

Manaoj Aravind, Sudeshna Sinha and P. Parmananda

Competitive interplay of repulsive coupling and cross-correlated noises in bistable systems

Cite as: Chaos **31**, 061106 (2021); doi: 10.1063/5.0056173
Submitted: 7 May 2021 · Accepted: 25 May 2021 ·
Published Online: 7 June 2021

Manaoj Aravind,[1,a)] Sudeshna Sinha,[2,b)] and P. Parmananda[1,c)]

AFFILIATIONS

[1] Department of Physics, Indian Institute of Technology Bombay, Powai, Mumbai 400 076, India
[2] Indian Institute of Science Education and Research Mohali, Knowledge City, SAS Nagar, Sector 81, Manauli, Punjab P.O. 140306, India

[a)] **Author to whom correspondence should be addressed:** manaojaravind@iitb.ac.in
[b)] **Electronic mail:** sudeshna@iisermohali.ac.in
[c)] **Electronic mail:** punit@phy.iitb.ac.in

ABSTRACT

The influence of noise on synchronization has potential impact on physical, chemical, biological, and engineered systems. Research on systems subject to common noise has demonstrated that noise can aid synchronization, as common noise imparts correlations on the sub-systems. In our work, we revisit this idea for a system of bistable dynamical systems, under repulsive coupling, driven by noises with varying degrees of cross correlation. This class of coupling has not been fully explored, and we show that it offers new counter-intuitive emergent behavior. Specifically, we demonstrate that the competitive interplay of noise and coupling gives rise to phenomena ranging from the usual synchronized state to the uncommon anti-synchronized state where *the coupled bistable systems are pushed to different wells*. Interestingly, this progression from anti-synchronization to synchronization goes through a domain where the system *randomly hops between the synchronized and anti-synchronized states*. The underlying basis for this striking behavior is that correlated noise preferentially enhances coherence, while the interactions provide an opposing drive to push the states apart. Our results also shed light on the robustness of synchronization obtained in the idealized scenario of perfectly correlated noise, as well as the influence of noise correlation on anti-synchronization. Last, the experimental implementation of our model using bistable electronic circuits, where we were able to sweep a large range of noise strengths and noise correlations in the laboratory realization of this noise-driven coupled system, firmly indicates the robustness and generality of our observations.

Coupled bistable systems provide a particularly simple, yet rich, platform to explore the interplay of noise and coupling. This is a problem that has garnered long-standing attention, as it has bearing on our basic understanding of the collective behavior of noise-driven coupled nonlinear systems and also offers opportunities for potential applications. For instance, it has been recently demonstrated that in the presence of attractive coupling, noise-induced transitions in such systems can synchronize, and this happens even when the noises driving the subsystems are uncorrelated. While most research efforts have focused on the constructive effect of noise in aiding synchronization, in this work, we explore systems coupled through repulsive interactions that may oppose the effect of noise, and we present the new implications of this competitive interplay of noise and coupling. The test-bed of our study is prototypical repulsively coupled bistable systems, subject to noises with different degrees of cross correlation. This allows us to explore the nontrivial interaction between repulsive coupling and noise, as well as ascertain the role of noise correlation in the synchronization of such noise-driven subsystems. We find that this system exhibits a rich variety of behavior including complete synchrony, complete antisynchrony, and a unique regime with windows of synchrony interspersed with antisynchrony. To reiterate, *anti-synchronization refers to the state when the bistable subsystems are pushed to different wells*. The behavior of this system is characterized over a large range of noise strengths and noise correlations, including a measure reflecting the random hopping between synchronized and anti-synchronized states. All observations are verified experimentally using electronic circuit experiments, indicating the robustness of our central results.

I. INTRODUCTION

Synchronization is a phenomenon that is widely observed in both natural and engineered systems. Typically, synchronization of dynamical subsystems is achieved either through coupling or through common external forcing.[1–4] The form of this coupling term may vary to produce interesting new phenomena; for instance, oscillation suppression through conjugate coupling,[5,6] phase flip transition due to time-delay coupling,[7,8] or multistability in repulsive coupling.[9,10] In another direction, interaction of noise with nonlinearity produces a wide variety of cooperative behavior.[11–14] A broad area of study where interaction with noise can play a pivotal role is in multistable systems, where noise-induced escape from locally stable attractors gives rise to novel phenomena such as stochastic resonance.[15] Noise has even been used as the common external forcing that brings about the onset of synchrony, in a phenomenon termed as noise-induced synchronization.[16–20]

The coupled systems governed by both noise and coupling exhibit interesting interplay between these two influences. While much work has focused on attractive coupling, both attractive and repulsive coupling are known to occur in natural systems. For instance, in neuroscience, attractive coupling can be related to excitatory synapses and repulsive coupling can be related to inhibitory synapses,[21] and repulsive coupling between circadian clock neurons in the suprachiasmatic nucleus is shown to encode seasonal time.[22] Repulsive coupling has also recently been found to be of importance in chemically active matter, giving rise to new phenomena such as anti-swarming.[23] Therefore, the interplay of repulsive coupling and noise is an important question that is currently gaining considerable attention.[24,25] Also, Nicolaou *et al.* have very recently reported that uncorrelated noise can be more effective than common noise in enhancing synchronization of coupled oscillators.[26] Connecting these two threads evokes the question: does noise correlation aid or inhibit synchronization in repulsively coupled systems, and does it lead to any qualitatively different behavior?

Studying noise-induced transitions in coupled bistable systems has the potential to make the interplay of noise and coupling clearly apparent, as the subsystems are simple and exhibit fixed point dynamics. This allows the activity of the subsystems to be viewed as transitions between the two "potential wells"; therefore, such systems can serve as a useful test-bed for the general understanding of the influence of correlated noise.[27,28] Furthermore, bistable systems are relevant in a variety of fields, ranging from relaxation oscillators and multivibrators to light switches and Schmitt triggers. Therefore, the study of noise-driven coupled bi-stable systems is also relevant from the standpoint of engineered systems with potential applications.[29]

Now, it has been shown that interplay of attractive coupling and uncorrelated noises in coupled bistable systems can induce synchronous escapes (hops) between locally stable wells for an optimal region in coupling and noise strengths.[30] In this work, we will focus on the interaction of repulsive coupling and cross-correlated noises in a coupled bistable system. We adopt a novel parameter, noise correlation coefficient (ρ), which allows us to smoothly vary the cross correlation between the noise experienced by the two subsystems. Both numerical simulations and electronic circuit experiments will be used to explore this system, and we expect the nontrivial interplay of correlated noises and repulsive coupling to produce a variety of novel behaviors.

II. MODEL

Consider a coupled bistable system (cf. Fig. 1) whose governing equations are of the form

$$\begin{aligned} \dot{x_1} &= F(x_1) + c(-x_2 - x_1) + D\,\eta_1(t), \\ \dot{x_2} &= F(x_2) + c(-x_1 - x_2) + D\,\eta_2(t). \end{aligned} \tag{1}$$

Here, F can be any nonlinear function that yields a bistable potential. We use the simple cubic function, $F(x_i) = 4(x_i - 5x_i^3)$, which gives rise to a bistable system with two stable fixed points $x_- = -1/\sqrt{5}$ and $x_+ = +1/\sqrt{5}$, separated by an unstable fixed point (the "barrier") at $x = 0$. The state characterized by positive valued state variables is denoted as the "positive well" and that characterized by negative valued state variables is denoted as the "negative well."

The coupling between the two subsystems is repulsive and bidirectional in nature. At a significant value of the coupling strength c, the coupling term causes the two subsystems to repel each other into opposite wells, namely, when x_1 is in the negative well and x_2 is in the positive well and vice versa.

Each subsystem is driven by a zero mean Gaussian noise with variance 1, and the parameter D denotes the strength of this noise. A characteristic feature of our model is that the noises η_1 and η_2 are cross-correlated with each other with a correlation coefficient ρ; i.e., if X_1 and X_2 are the two Gaussian random variables used to generate these noises (η_1 and η_2), then ρ is given as

$$\rho_{X_1,X_2} = \frac{\langle (X_1 - \langle X_1 \rangle)(X_2 - \langle X_2 \rangle) \rangle}{\sigma^2}. \tag{2}$$

It is important to note that the noise sequences η_1 and η_2 are *generated* with this specific cross correlation. Therefore, the measure ρ acts as an additional parameter in our model that fixes the amount of the correlation between η_1 and η_2. When $\rho = 0$, the two noises are completely independent and uncorrelated. $\rho = 1$ implies that the two noises are exactly the same ($\eta_1 = \eta_2$), i.e., common noise. Thus, ρ provides a parameter to smoothly vary the extent of the correlation between the two noise sequences from uncorrelated noise to common noise.

The only force driving the subsystems is the two noise terms η_1 and η_2. Hence, the only dynamics the subsystems exhibit are the noise-induced transitions (over the barrier) from one potential well to the other. Therefore, the study of coupled bistable systems driven by noise implies a study of synchrony of these noise-induced transitions. It is well documented that common noise synchronizes

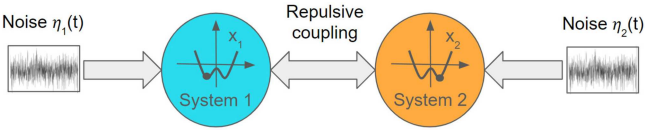

FIG. 1. A schematic representation of the model.

nonlinear subsystems,[16–20] while large uncorrelated noise is expected to inhibit synchronization. Thus, in a system driven purely by noise, the parameter ρ allows us to precisely vary the effect that these noises have on system dynamics, thereby allowing for both synchrony and asynchrony in these noise-induced transitions.

We explore the behavior of our coupled bistable model by varying these three system parameters (in the parameter range $c \in [0, 3]$, $D \in [0, 1]$, and $\rho \in [0, 1]$). The coupling strength c fixes the amount of repulsive interactions between the subsystems. The noise strength D and the noise correlation ρ determine the strength and nature of the stochastic forcing, driving the subsystems. A rich variety of behavior ranging from complete antisynchrony induced by the repulsive coupling to complete synchrony produced by common noise is observed in this model. The various behaviors observed and their characterization are detailed in Sec. III.

III. RESULTS

To showcase the multitude of behaviors seen, we first display results from the numerical simulation of stochastic differential equations that describe the system [cf. Eq. (1)]. These simulations were performed using the Euler–Maruyama method with a stepsize of 10^{-2}. In Fig. 2, time trails of the state variables x_1 (blue) and x_2 (orange) are plotted for different values of system parameters (the exact values are indicated above each panel). Along with x_1 and x_2, the absolute difference between the two variables $|x_1 - x_2|$ (green) is also plotted as a visual aid to gauge the amount of synchrony between the x_1 and x_2 time trails. On the right side of each panel is a normalized histogram measured over long simulation times (2×10^5 time steps), depicting the distribution of these $|x_1 - x_2|$ values. All plots in Fig. 2 are simulated for coupling strength $c = 1$, which is a moderate value that allows diverse behavior.

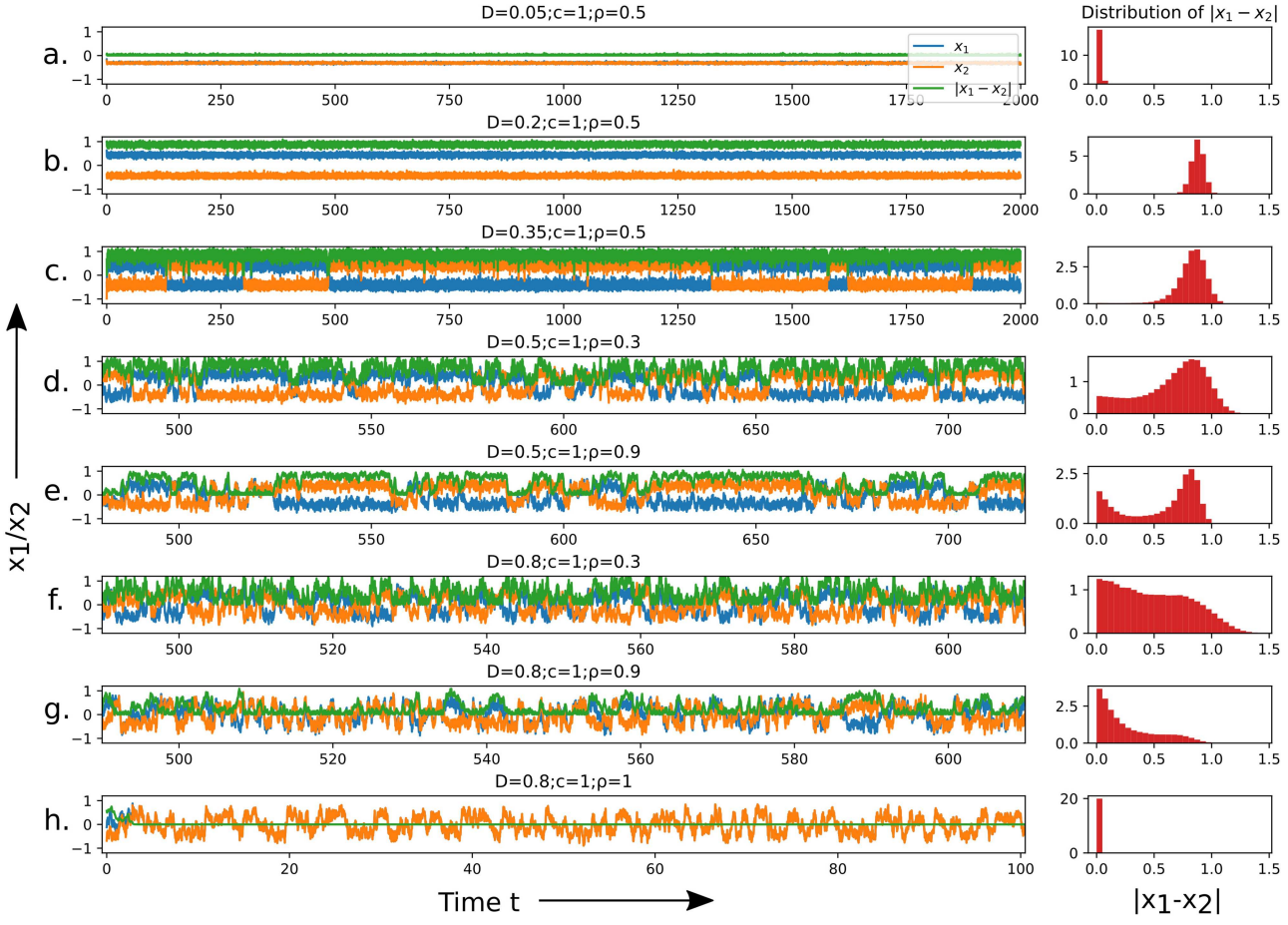

FIG. 2. Time trails of the two system variables x_1 (blue) and x_2 (orange) and their absolute difference $|x_1 - x_2|$ (green) obtained by simulating Eq. (1) for a range of parameter values. The specific parameter values corresponding to each plot from top to bottom are as follows: (a) $D = 0.05$, $c = 1$, $\rho = 0.5$; (b) $D = 0.2$, $c = 1$, $\rho = 0.5$; (c) $D = 0.35$, $c = 1$, $\rho = 0.5$; (d) $D = 0.5$, $c = 1$, $\rho = 0.3$; (e) $D = 0.5$, $c = 1$, $\rho = 0.9$; (f) $D = 0.8$, $c = 1$, $\rho = 0.3$; (g) $D = 0.8$, $c = 1$, $\rho = 0.9$; and (h) $D = 0.8$, $c = 1$, $\rho = 1$. Here, D, c, and ρ denote noise strength, coupling strength, and noise correlation coefficient, respectively. On the right end of each panel is the normalized histogram depicting the distribution of $|x_1 - x_2|$ values obtained by simulating the corresponding time trails for a long simulation time (2×10^5 timesteps).

The top panel [Fig. 2(a)] corresponds to the case when noise strength D is very small ($D = 0.05$). Thus, in spite of the repulsive coupling, the two subsystems simply stay in the potential wells determined by their initial condition; i.e., they may begin in the same well or in opposite wells and continue in that stable state. The next two panels [Figs. 2(b) and 2(c)] show the system response for low noise strengths ($D = 0.2$ and $D = 0.35$) and moderate coupling strength ($c = 1$). Here, the noise strength is enough to facilitate the transition between the potential wells, and the two subsystems are robustly pushed to opposite wells because of the repulsive coupling. It is interesting to note that a small amount of noise is necessary to facilitate the interaction between the subsystems for moderate coupling strengths. These trajectories clearly show the *antisynchrony induced by repulsive coupling between the subsystems*. Also, in both Figs. 2(b) and 2(c), $|x_1 - x_2| \approx 0.9$ for all time, which clearly denotes robust antisynchrony.

The fourth and fifth panel [Figs. 2(d) and 2(e)] correspond to moderate values of noise strength ($D = 0.5$) and coupling strength ($c = 1$). In this regime, noises in the subsystems are strong enough to overcome the antisynchrony caused by the repulsive coupling. Windows of a noise-induced activity (transitions between the potential wells) are seen in between phases of antisynchrony caused by the repulsive coupling. This can be clearly seen by following the intermittent rise and fall of the $|x_1 - x_2|$ plots (green) in the corresponding time trails. This alternation in time clearly shows the rich interplay between repulsive coupling and noise in our model. It is very interesting to note that these windows of noise-induced activity are highly synchronized for the case of a high noise correlation [cf. Fig. 2(e)], i.e., for $\rho = 0.9$. This can be inferred from the corresponding histogram that shows two sharp peaks, one about $|x_1 - x_2| \approx 0.9$, corresponding to the antisynchronous windows, and the other about $|x_1 - x_2| = 0$ corresponding to the highly synchronous windows caused by the highly correlated noises. It is this unique behavior, where *synchrony and antisynchrony coexist and temporally alternate*, that we want to highlight among the plethora of possibilities within this model. We would like to point out that these switches are reminiscent of phase-flips. The fact that both phases can coexist points to the emergence of multistability due to the competing influences of repulsive coupling and highly correlated noise. The switch between these two phases is brought about by the stochasticity inherent in this model. Hence, we term these alternations *stochastic phase-flips*. In contrast to the fifth panel, the noise-induced activity in the fourth panel [Fig. 2(d)], i.e., for the case of a low noise correlation ($\rho = 0.3$), is not synchronized. This can also be understood from the corresponding histogram through the clear absence of a prominent peak about $|x_1 - x_2| = 0$. Hence, we deduce that these continuous flips between the antisynchronous and synchronous modes are the result of *competing influences from repulsive coupling and highly cross-correlated noises*, respectively.

The sixth and seventh panels [Figs. 2(f) and 2(g)] correspond to high noise strength ($D = 0.8$) and moderate coupling strength ($c = 1$). The sixth panel [Fig. 2(f)] shows the timetrails for a low noise correlation ($\rho = 0.3$) and the seventh panel [Fig. 2(g)] for a high noise correlation ($\rho = 0.9$). Here, due to high noise strength, noise-induced transitions dominate most of the time. The effect of repulsive coupling is barely seen in the small antisynchronous windows that arise in between. This can also be inferred from the flattening of the peak corresponding to antisynchrony (the peak about $|x_1 - x_2| \approx 0.9$) from histograms of both timetrails. It is again seen both from the time trail and histogram of the seventh panel [Fig. 2(g)] that the noise-induced transitions are highly synchronous when the cross correlation between the two noises are high ($\rho = 0.9$). Conversely, the sixth panel shows noise dominated trajectories with very less correlations as seen from the broad unimodality of the corresponding histogram. Thus, both the fifth and seventh panel point toward the idea that a high noise correlation clearly leads to improved synchrony even if the coupling term is repulsive.

The eighth panel [Fig. 2(h)] corresponds to the limiting case where a noise correlation $\rho = 1$; i.e., the two subsystems are driven by the exact same noise sequence. For the case of common noise, the subsystems always stabilize to completely synchronized transitions between the two potential wells. This again is made apparent by the singular peak at $|x_1 - x_2| = 0$ in the histogram.

Now that the different regimes of behavior in this model have been elucidated, we depict how these regimes are distributed in the parameter space. Given that our behavioral regimes are characterized by the amount of synchrony they exhibit, we rigorously quantify the synchrony between the two subsystems using a variant of synchronization error Z. Since our model is purely driven by noise, describing synchronization error as the deviation from complete synchronization leads to the requirement of an arbitrary threshold to denote synchronization (as the absolute values of these noise-driven trajectories may never completely overlap). Alternatively, we view the dynamics of our coupled bistable system as a series of transitions from one potential well to the other. Then, we can simply define the synchronization error as the fraction of time (measured over long simulation times) spent by the two subsystems in different potential wells. Since the potential barrier of our bistable system lies at $x = 0$, the product of the state variables is always negative when the subsystems are in different wells. Hence, synchronization error Z is easily defined mathematically as

$$Z = \frac{1}{N}\sum_{i=1}^{N} H(x_1[i] \times x_2[i]), \tag{3}$$

where N is the total number of timesteps in the observed time series, with N being very large, and H is given as

$$H(x_i) = \begin{cases} 1, & x_i < 0, \\ 0, & x_i \geq 0. \end{cases} \tag{4}$$

Figure 3 depicts this synchronization error Z as a heatmap over noise strength D and noise correlation ρ. Note that each plot in Fig. 3 corresponds to one value of coupling strength (indicated above each plot). The synchronization error Z [cf. Eqs. (3) and (4)] for each parameter value has been calculated by simulating Eq. (1) for 2×10^5 timesteps, leaving 2×10^3 timesteps as transients. Z corresponding to each parameter value combination has been averaged over 100 different initial conditions chosen randomly from the interval $[-1, 1]$. Each heatmap depicts the Z value corresponding to 1600 parameter (D and ρ) combinations.

In Fig. 3, for coupling constant $c = 1$, the parameter values corresponding to time trails in Fig. 2 have been marked over the heatmap. To identify and intuitively infer the various regimes of

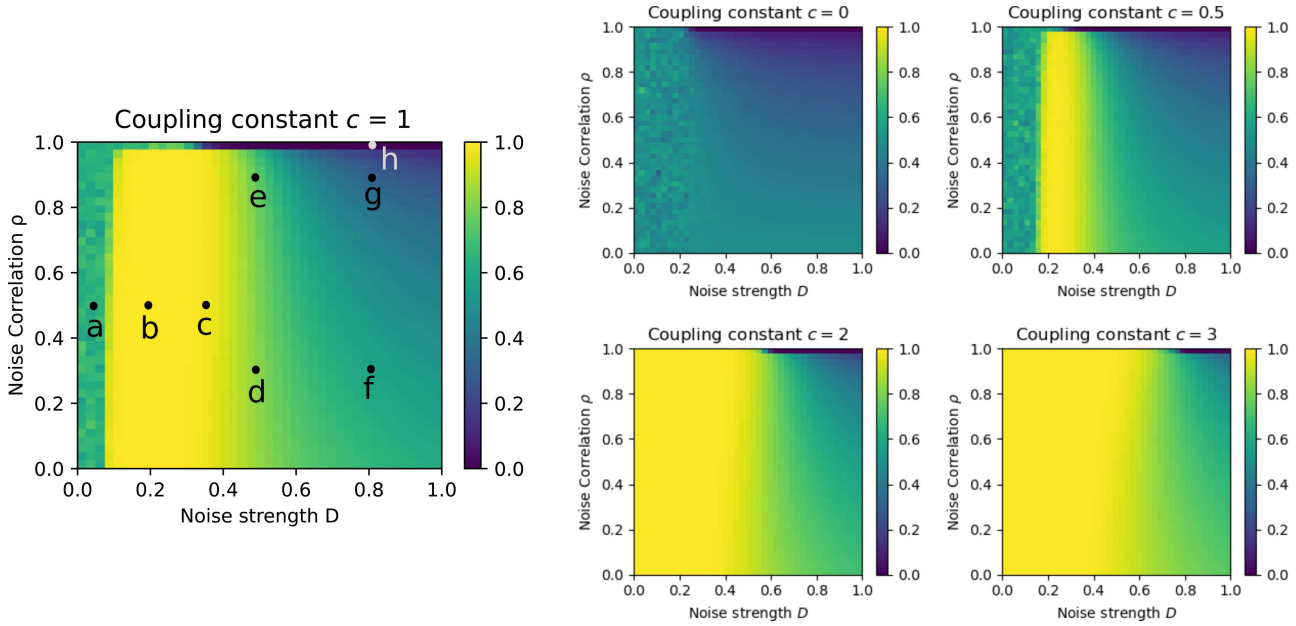

FIG. 3. Synchronization error Z [cf. Eq. (3)] plotted vs noise strength D and noise correlation ρ for various values (indicated above each plot) of coupling strength c. The parameter values of all the timetrails in Fig. 2 are marked on the $c = 1$ plot. We clearly see that as the strength of the repulsive coupling increases, the fraction of parameters yielding anti-synchrony increases.

behavior in the parameter space, we explore the heatmap of $c = 1$ in detail. For very low noise strengths $D < 0.07$, there is a region in the parameter space where the Z values are completely stochastic; i.e., the state variables are only dependent on the initial conditions. The parameter corresponding to Fig. 2(a) lies in this region. Beyond a critical noise strength ($0.07 \leq D < 0.4$), a bright band of yellow, which represents $Z \simeq 1$, appears. This is the regime of complete antisynchrony, implying that repulsive coupling dominates the behavior in this region. The parameters corresponding to Figs. 2(b) and 2(c) lie here. Note that in this region, complete antisynchrony occurs for all values of noise correlation (except $\rho = 1$); i.e., this regime is unaffected by changes to the noise correlation. It is altered only by common noise ($\eta_1 = \eta_2$). Next is the region of moderate noise strength ($0.4 \leq D < 0.6$), which marks the fall of synchronization error Z from 1; i.e., this is the transition region where a noise-induced activity begins to appear in between windows of antisynchrony. The parameters corresponding to Figs. 2(d) and 2(e) appear here. Beyond $D \geq 0.6$ is the region of high noise strength where the behavior of the system is dominated by noise. The parameters corresponding to Figs. 2(f) and 2(g) occur here. In this region, there exists a gradient of synchronization error Z as the noise correlation coefficient ρ goes from zero to one. For a lower noise correlation, $Z \approx 0.5$ meaning that the state variables in this region are mostly uncorrelated. As ρ approaches one, Z approaches zero, which demonstrates the constructive role of noise correlation in the onset of synchrony. The region with the points "e" and "g," i.e., the region with sufficient noise strength, coupling strength, and high noise correlation, is where continuous flips between synchrony and antisynchrony occur.

These regimes characterized by Z exist across all the different values of coupling strengths. For $c = 0$, there is no region of antisynchrony (bright yellow) as there is no repulsive coupling. As the value of coupling strength c is increased ($c = 0.5$ and $c = 1$), a region of complete antisynchrony appears for an optimal range of noise strengths. For higher values of c ($c = 2$ and $c = 3$), antisynchrony dominates over most of the parameter space. For the case of $\rho = 1$, i.e., for common noise, the subsystems completely synchronize beyond a critical value of noise strength. This is true for all the studied values of coupling strength. The parameter value for Fig. 2(h) lies in this region of complete synchrony on the $c = 1$ heatmap. Thus, we have thoroughly explored the various behaviors of this system across a large section of the parameter space. In Sec. IV, experimental validation of all simulation results is detailed.

IV. EXPERIMENTAL IMPLEMENTATION

The study of noise-driven multistable systems has wide real world applications, from modeling chemical kinetics[31,32] to designing noise-aided logic gates.[29,33–35] Hence, it is all the more important to experimentally demonstrate the generality of our observations. To do this, we implement the same model described in Sec. II, now with a simple bistable electronic circuit. Specifically, we use a piecewise linear circuit that can be constructed with very few components and can be robustly reproduced to make identical coupled units. The non-dimensionalized form of the coupled circuit equation becomes

$$\begin{aligned} \dot{x_1} &= F(x_1) + c(-x_2 - x_1) + D\,\eta_1(t), \\ \dot{x_2} &= F(x_2) + c(-x_1 - x_2) + D\,\eta_2(t), \end{aligned} \tag{5}$$

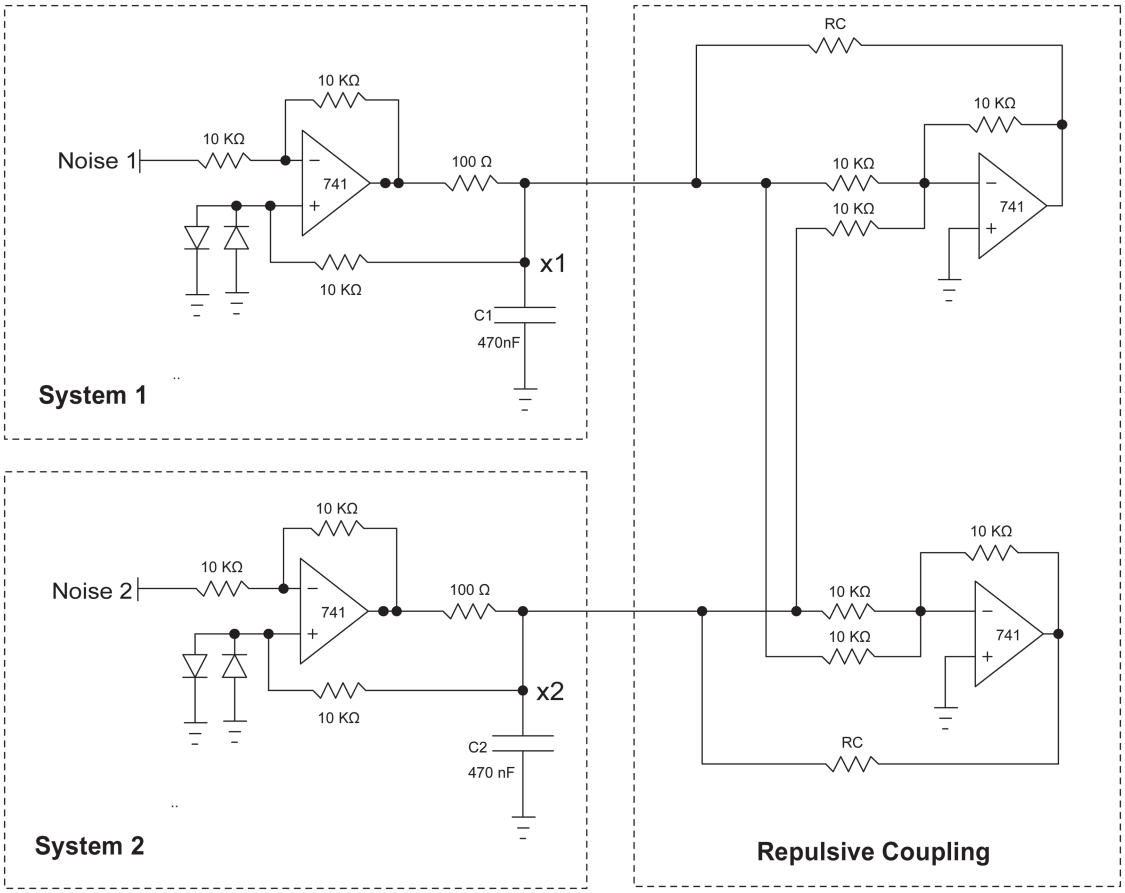

FIG. 4. The schematic circuit diagram of the experimental setup. All component values are indicated on the diagram. The diodes used in the circuit are 1N4148 diodes. We study the circuit for two values of coupling resistances, $R_C = 1200\ \Omega$ and $R_C = 300\ \Omega$. The system variables x_1 and x_2 from Eq. (5) are proportional to voltages V_1 and V_2 across C_1 and C_2.

where F is a piecewise linear function given by

$$F(x_i) = \begin{cases} -(x_i + 1), & x_i < -0.5, \\ x_i, & -0.5 \le x_i \le 0.5, \\ -(x_i - 1), & x_i > 0.5. \end{cases} \tag{6}$$

A schematic representation of the coupled circuit is given in Fig. 4. The full details of implementing this nonlinearity F are discussed in Ref. 36. From Fig. 4, we see that the two state variables of this electronic implementation are the voltages V_1 and V_2 across the capacitors C_1 and C_2. All the specific component values used in the construction of the circuit are indicated in the schematic. The two bistable subsystems (marked in the schematic) have been coupled through two op-amp adder circuits. The inverted sum of the two state variables obtained from these adders provides the necessary functional form for repulsive coupling. All oscilloscope trails were obtained using a Tektronics 2104B digital storage oscilloscope. A Measurement Computing (USB-1616HS) high speed data acquisition device was used to both generate the correlated Gaussian noises of specific noise correlations and also to record all experimental voltage time-series data for further analysis.

Figure 5 shows the oscilloscope traces for various values of system parameters. Here, again (as in Fig. 2), we clearly see the different regimes of behavior detailed in Sec. III. Panel 4 [Fig. 5(d)] clearly shows the windows of noise-induced synchrony in between antisynchrony caused by repulsive coupling. It is interesting to note that even when $\rho = 1$ [as in Fig. 5(f)], complete synchronization does not occur in experimental systems. This is to be expected because perfectly identical systems cannot be experimentally constructed and also identical driving forces can never be generated. Thus, instead of complete synchrony, at $\rho = 1$, the system demonstrates a behavior similar to Fig. 2(g). This points to the crucial detail that *the behavior of our model with a very high noise correlation is more relevant in real systems than perfectly common noise*, thereby eliciting the importance of this work.

Thus, all the behavioral regimes observed in simulation have been experimentally shown. We further reinforce our findings through the complete characterization of experimental time-series

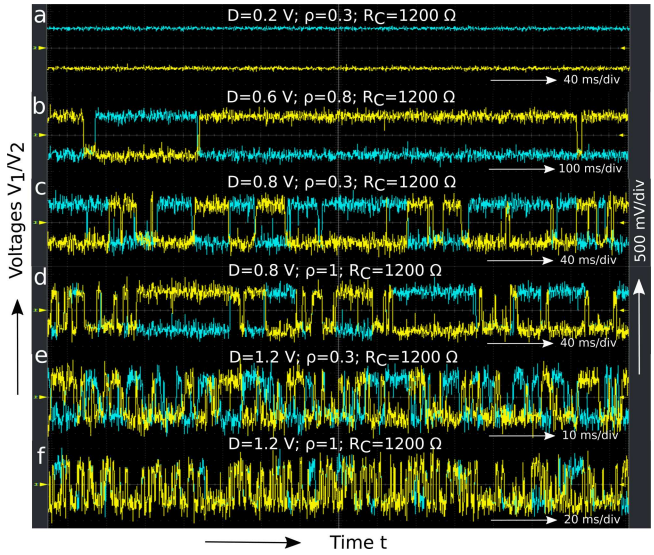

FIG. 5. Oscilloscope traces of voltages V_1 (blue) and V_2 (yellow) across capacitors C_1 and C_2 (cf. Fig. 4) obtained for various values of system parameters. The specific parameter values corresponding to each trail from top to bottom are as follows: (a) $D = 0.2$ V, $\rho = 0.3$, $R_C = 1200\,\Omega$, (b) $D = 0.6$ V, $\rho = 0.8$, $R_C = 1200\,\Omega$, (c) $D = 0.8$ V, $\rho = 0.3$, $R_C = 1200\,\Omega$, (d) $D = 0.8$ V, $\rho = 1$, $R_C = 1200\,\Omega$, (e) $D = 1.2$ V, $\rho = 0.3$, $R_C = 1200\,\Omega$, and (f) $D = 1.2$ V, $\rho = 1$, $R_C = 1200\,\Omega$. Here, D denotes noise amplitude, ρ denotes noise correlation, and R_C denotes coupling resistance (cf. Fig. 4). The various regimes of behavior observed in Fig. 2 are clearly seen here in the experimental timetrails.

data measured using a high speed data acquisition device. The voltages V_1 and V_2 were measured for 10 s at a sample rate of 2×10^5 data points per second. Ten such samples each for 150 parameter value combinations were recorded. These data were then used to calculate synchronization error Z [cf. Eqs. (3) and (4)] for all parameter values. The experimental data were recorded for two specific values of coupling resistance R_c, namely, 1200 and 300 Ω. The experimental parameter space plot thus obtained is shown in Fig. 6. Parameter values for the oscilloscope traces in Fig. 5 are overlaid on the parameter space plot in Fig. 6. We again see complete correspondence with our numerical characterization.

V. SUMMARY AND DISCUSSION

The behavior of repulsively coupled bistable elements driven only by noise was explored in detail. We scanned the space of three parameters: coupling strength c, noise strength D, and noise correlation coefficient ρ. A wide range of behavior from complete antisynchrony to complete synchrony was observed. A new kind of behavior involving continuous alternations between synchronous and antisynchronous modes was found both in simulations and electronic circuit experiments. The different behaviors observed were characterized using a new measure of synchronization that reflects the propensity of two coupled bistable sub-systems to be attracted to the same potential well. All aspects of our numerical study, including the detailed characterization in the parameter space, were also reproduced through electronics. It is important to note here that the challenge of the experimental verification lies in the implementation of a sweep of noise strengths and noise correlations, which is

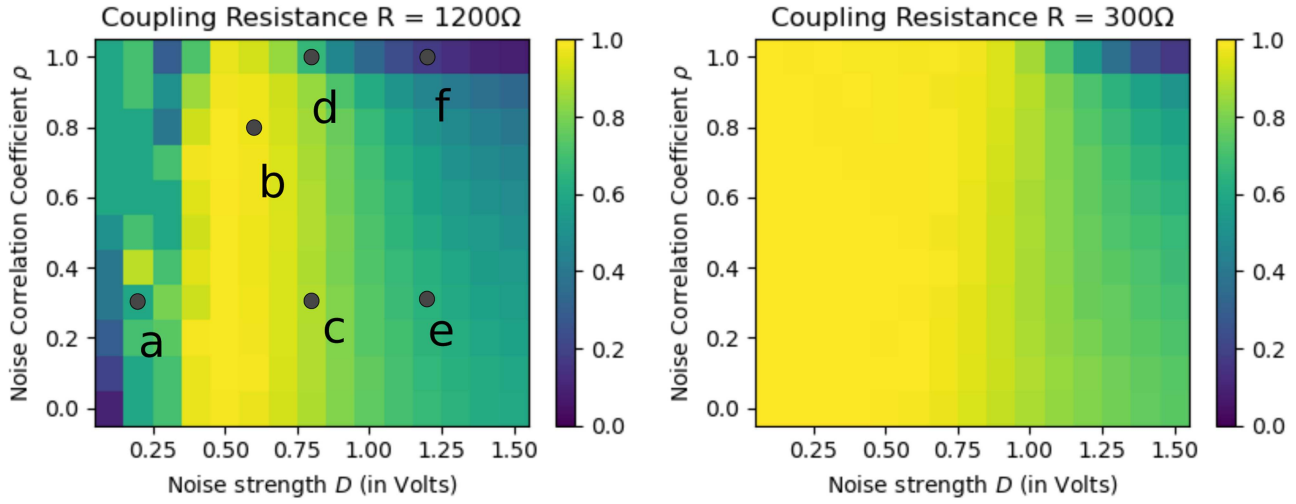

FIG. 6. Synchronization error Z, computed from experimental data, recorded using a high speed data acquisition device (Measurement Computing USB-1616HS). Z is plotted here vs noise strength D and noise correlation coefficient ρ. Left: For coupling resistance, $R_C = 1200\,\Omega$. The parameter values of the time trails in Fig. 5 are marked. Right: For coupling resistance, $R_C = 300\,\Omega$.

typically difficult. Most reported experimental results present a few specific noise strengths and noise correlations, but not the full range. We have managed to efficiently set up a fine sweep, and therefore, our experiments were capable of providing a stringent, detailed, and comprehensive verification of the numerical results.

Our study elaborates the interesting competing interplay between repulsive coupling and cross-correlated noises. All coupled systems that share a physical environment experience noises that are correlated to some degree. While such environmental fluctuations in physically contiguous systems are expected to have some degree of cross correlation, it is unlikely to have perfect correlations. It is in this context that this work gains relevance, as we present a way to model these regimes of intermediate correlations and also describe unique behaviors that arise in those regimes.

As demonstrated in the experimental observations, forcing with highly correlated noise, in other words "almost common forcing," is of more real world relevance than perfect common noise whose correlation is exactly one. Certain outcomes generated by perfectly correlated common noise in numerical simulations, such as complete synchronization in a noise window for all repulsive coupling strengths, are not robust to small loss in the noise correlation; i.e., the behavior is lost when noise correlation coefficient ρ is even slightly less than one. Therefore, various behaviors may be more of an exception than the norm, as they occur only in the limit of a perfect correlation. This points to the importance of the present study from the broad standpoint of modeling noise-induced behavior in coupled systems, as we demonstrate how noise correlations may play a key role in the observability of emergent behavior in real systems.

ACKNOWLEDGMENTS

We are grateful for the support provided by DST [Grant No. EMR/2016/000275 (P.P.)]. This work was supported by the Department of Physics, IIT Bombay.

DATA AVAILABILITY

The data that support the findings of this study are available from the corresponding author upon reasonable request.

REFERENCES

[1]A. Pikovsky, J. Kurths, M. Rosenblum, and J. Kurths, *Synchronization: A Universal Concept in Nonlinear Sciences* (Cambridge University Press, 2003), Vol. 12.
[2]Y. Kuramoto, in *International Symposium on Mathematical Problems in Theoretical Physics* (Springer, 1975), pp. 420–422.
[3]D. K. Verma, H. Singh, A. Contractor, and P. Parmananda, J. Phys. Chem. A **118**, 4647 (2014).
[4]D. K. Verma, H. Singh, P. Parmananda, A. Contractor, and M. Rivera, Chaos **25**, 064609 (2015).
[5]M. Dasgupta, M. Rivera, and P. Parmananda, Chaos **20**, 023126 (2010).
[6]T. Singla, N. Pawar, and P. Parmananda, Phys. Rev. E **83**, 026210 (2011).
[7]A. Prasad, J. Kurths, S. K. Dana, and R. Ramaswamy, Phys. Rev. E **74**, 035204 (2006).
[8]J. Cruz, J. Escalona, P. Parmananda, R. Karnatak, A. Prasad, and R. Ramaswamy, Phys. Rev. E **81**, 046213 (2010).
[9]S. Astakhov, A. Gulai, N. Fujiwara, and J. Kurths, Chaos **26**, 023102 (2016).
[10]Z. Levnajić, Phys. Rev. E **84**, 016231 (2011).
[11]J. Escorcia-Garcia, V. Agarwal, and P. Parmananda, Appl. Phys. Lett. **94**, 133103 (2009).
[12]M. Rivera, G. J. E. Santos, J. Uruchurtu-Chavarin, and P. Parmananda, Phys. Rev. E **72**, 030102 (2005).
[13]M. Nurujjaman, A. S. Iyengar, and P. Parmananda, Phys. Rev. E **78**, 026406 (2008).
[14]G. J. E. Santos, M. Rivera, J. Escalona, and P. Parmananda, "Interaction of noise with excitable dynamics," Philos. Trans. R. Soc. London, Ser. A **366**, 369–380 (2008).
[15]L. Gammaitoni, P. Hänggi, P. Jung, and F. Marchesoni, Rev. Mod. Phys. **70**, 223 (1998).
[16]A. Maritan and J. R. Banavar, Phys. Rev. Lett. **72**, 1451 (1994).
[17]C. Zhou, J. Kurths, I. Z. Kiss, and J. L. Hudson, Phys. Rev. Lett. **89**, 014101 (2002).
[18]D. S. Goldobin and A. Pikovsky, Physica A **351**, 126 (2005).
[19]J. Teramae and D. Tanaka, Phys. Rev. Lett. **93**, 204103 (2004).
[20]I. Z. Kiss, J. L. Hudson, J. Escalona, and P. Parmananda, Phys. Rev. E **70**, 026210 (2004).
[21]Q. Wang, G. Chen, and M. Perc, PLoS One **6**, e15851 (2011).
[22]J. Myung *et al.*, Proc. Natl. Acad. Sci. U.S.A. **112**, E3920 (2015).
[23]W. Yan and J. Brady, Phys. Rev. E **96**, 060601 (2017).
[24]A. V. Pimenova, D. S. Goldobin, M. Rosenblum, and A. Pikovsky, Sci. Rep. **6**, 38518 (2016).
[25]C. C. Gong, C. Zheng, R. Toenjes, and A. Pikovsky, Chaos **29**, 033127 (2019).
[26]Z. G. Nicolaou, M. Sebek, I. Z. Kiss, and A. E. Motter, Phys. Rev. Lett. **125**, 094101 (2020).
[27]P. D. Rungta, A. Choudhary, C. Meena, and S. Sinha, Europhys. Lett. **117**, 20003 (2017).
[28]P. D. Rungta, C. Meena, and S. Sinha, Phys. Rev. E **98**, 022314 (2018).
[29]K. Murali, S. Sinha, W. L. Ditto, and A. R. Bulsara, Phys. Rev. Lett. **102**, 104101 (2009).
[30]V. M. Aravind, K. Murali, and S. Sinha, in *Nonlinear Dynamics and Control* (Springer, 2020), pp. 325–334.
[31]J. M. Cruz, P. Parmananda, and T. Buhse, J. Phys. Chem. A **112**, 1673 (2008).
[32]S. Sinha, J. Cruz, T. Buhse, and P. Parmananda, Europhys. Lett. **86**, 60003 (2009).
[33]M. Aravind, K. Murali, and S. Sinha, Phys. Lett. A **382**, 1581 (2018).
[34]K. Murali, S. Sinha, V. Kohar, B. Kia, and W. L. Ditto, PLoS One **13**, e0209037 (2018).
[35]K. Murali, S. Rajasekar, M. V. Aravind, V. Kohar, W. Ditto, and S. Sinha, "Construction of logic gates exploiting resonance phenomena in nonlinear systems," Philos. Trans. R. Soc. London, Ser. A **379**(2192), 20200238 (2021).
[36]E. Adomaitienė, A. V. Tamaševičius, G. Mykolaitis, S. Bumelienė, and E. Lindberg, Nonlinear Anal. Model. Control **13**, 241 (2008).